



**HAL**  
open science

## Designing Large Two-Dimensional Arrays of Josephson Junctions for RF Magnetic Field Detection

Denis Gérard Crété, Sarah Menouni, Juan Trastoy, Salvatore Mesoraca, Julien Kermorvant, Yves Lemaître, Bruno Marcilhac, Christian Ulysse

► **To cite this version:**

Denis Gérard Crété, Sarah Menouni, Juan Trastoy, Salvatore Mesoraca, Julien Kermorvant, et al.. Designing Large Two-Dimensional Arrays of Josephson Junctions for RF Magnetic Field Detection. Electronics, 2023, 12 (15), pp.3239. 10.3390/electronics12153239 . hal-04611701

**HAL Id: hal-04611701**

**<https://hal.science/hal-04611701>**

Submitted on 13 Jun 2024

**HAL** is a multi-disciplinary open access archive for the deposit and dissemination of scientific research documents, whether they are published or not. The documents may come from teaching and research institutions in France or abroad, or from public or private research centers.

L'archive ouverte pluridisciplinaire **HAL**, est destinée au dépôt et à la diffusion de documents scientifiques de niveau recherche, publiés ou non, émanant des établissements d'enseignement et de recherche français ou étrangers, des laboratoires publics ou privés.



Distributed under a Creative Commons Attribution 4.0 International License

## Article

# Designing Large Two-Dimensional Arrays of Josephson Junctions for RF Magnetic Field Detection

Denis Gérard Crété <sup>1,\*</sup>, Sarah Menouni <sup>1</sup>, Juan Trastoy <sup>1</sup>, Salvatore Mesoraca <sup>1</sup>, Julien Kermorvant <sup>2</sup>, Yves Lemaître <sup>1,†</sup>, Bruno Marcilhac <sup>1,†</sup> and Christian Ulysse <sup>3</sup>

<sup>1</sup> Unité Mixte de Physique CNRS/THALES, University Paris-Saclay, 91767 Palaiseau, France; sarah.menouni@thalesgroup.com (S.M.); juan.trastoy@thalesgroup.com (J.T.); salvatore.mesoraca@thalesgroup.com (S.M.); yves.lemaître@cnrs-thales.fr (Y.L.); bruno.marcilhac@cnrs-thales.fr (B.M.)

<sup>2</sup> THALES SIX, 92230 Gennevilliers, France; julien.kermorvant@thalesgroup.com

<sup>3</sup> Centre for Nanoscience and Nanotechnology, CNRS, Université Paris-Saclay, 91140 Palaiseau, France; christian.ulyссе@c2n.upsaclay.fr

\* Correspondence: denis.crete@thalesgroup.com; Tel.: +33-1-69-41-58-52

† Now retired.

**Abstract:** This paper discusses improved design of two-dimensional (2D) arrays, potentially pushing the present state of the art of the high- $T_c$  (and low- $T_c$ ) magnetic field detectors to a larger scale, i.e., higher sensitivity. We propose a two-plate geometry for parallel (and two-dimensional) arrays of Josephson junctions (JJs) for application in magnetic field detection. The arrays can be realized either by integration in the same substrate with a multilayer technology or on two different substrates. In the latter case, the substrates can be assembled in a flip-chip or piggyback configuration. A suggestion would be to divide a 2D array in two (equal) parts and to distribute each part on a different layer, one above the other. We model the current distribution in arrays connected in series so that the bias current flowing through the device flows in opposite direction in the layers. We demonstrate that this geometry greatly improves the uniformity of the bias current distribution across the width of the array, thereby restoring the critical current and, in principle, improving the Josephson array response. From the model, we conclude that the alignment of the arrays is not critical and that the realization of the devices requires only conventional techniques.

**Keywords:** Josephson junction; superconducting quantum interference devices; magnetometer; dynamic; current distribution; parallel array; self-field; uniformity



**Citation:** Crété, D.G.; Menouni, S.; Trastoy, J.; Mesoraca, S.; Kermorvant, J.; Lemaître, Y.; Marcilhac, B.; Ulysse, C. Designing Large Two-Dimensional Arrays of Josephson Junctions for RF Magnetic Field Detection. *Electronics* **2023**, *12*, 3239. <https://doi.org/10.3390/electronics12153239>

Academic Editor: Michael I. Faley

Received: 24 May 2023

Revised: 20 July 2023

Accepted: 21 July 2023

Published: 26 July 2023



**Copyright:** © 2023 by the authors. Licensee MDPI, Basel, Switzerland. This article is an open access article distributed under the terms and conditions of the Creative Commons Attribution (CC BY) license (<https://creativecommons.org/licenses/by/4.0/>).

## 1. Introduction

In the domain of magnetic field detection, superconducting devices offer both a very high sensitivity and a large bandwidth. These detectors are mainly based on superconducting quantum interference devices (SQUIDs), which comprise a superconducting loop containing one or two Josephson junctions (JJs) [1–4]. They can be made of a large number of JJs, with several advantages in many applications [5]. For magnetic field detection, using arrays of JJs increases the detector transfer factor and dynamic range [6]. A flux-locked loop added to a single SQUID is a much-employed solution but at the expense of bandwidth limitation [7]. At radio frequencies, impedance matching is an important requirement to achieve good signal coupling. An array of  $N$  SQUIDs connected in series has an impedance scaling of  $N$ , thereby limiting  $N$  when the impedance becomes too large for a standard 50  $\Omega$  load [8]. The impedance of bidimensional arrays can be lowered by the addition of more JJs in parallel. In this case, the array becomes wider, and its transfer factor increases linearly with its width. This is true only if the bias current distribution is reasonably uniform. This requirement is not met for devices—either parallel arrays, 2D arrays or series arrays of long Josephson junctions (LJJs)—with a width in excess of about 100  $\mu\text{m}$  [9]. In this range, the

transfer factor collapses. In this study, we demonstrate bias current uniformity in a parallel array thanks to the Meissner effect. Magnetic induction ( $B$ ) is generated by the bias current ( $I_{bias}$ ) flowing in the array. Section 2 presents the principle of current distribution in a grid made of several superconducting parallel strips (or, equivalently, “branches”). Section 3 describes the model. Section 4 presents the results for a conventional technology and for nanocircuits. We discuss the results of this study and possible extrapolations in Section 5, and finally, Section 6 summarizes this article.

## 2. Principle

A superconductor is not only a perfect conductor with a vanishing electric field in its bulk but also expels the magnetic field because of the Meissner effect. This behavior is comparable to the very limited penetration of the RF electromagnetic field in a normal conductor; besides its frequency dependence, the skin depth is nearly equivalent to the London penetration depth ( $\lambda$ ). Consequently, we observe comparable field distributions in systems of normal conductors at RF and in systems of superconductors independent of the frequency. For normal conductors, it is well known that a single strip (with width  $W$ ) carries most of the current on its edges. Oswald [10] analyzed a geometry closer to that of a parallel array, i.e., a single planar grid of parallel superconducting wires, showing that the current distribution is strongly peaked for the wires located on both edges of the grid. The peak can be twice as large as the average current in the grid branches. This is consistent with the distribution observed in a wide superconducting strip.

In a microstrip structure, the strip current distribution is much more uniform. We modeled this distribution for a superconducting microstrip structure in a previous paper [11] and showed that the current distribution in the ground plane was confined in the vicinity of the strip within a range of the strip width ( $W$ ). The current distribution in the 10  $\mu\text{m}$ -wide superconducting strip departed from perfect uniformity by only 20% with a ground plane at a distance  $z_h = 0.15 \mu\text{m}$  from the strip, while it was about 70% when  $z_h = 5 \mu\text{m}$ . As JJs are highly non-linear devices with a threshold at the critical current, such non-uniformity in the current distribution is detrimental: the critical current of the device is no longer the sum of the individual branch critical currents, but it reaches a limit as for LJJs [12]. For a long Josephson junction, this limit is reached when a Josephson vortex can penetrate the LJJ. This may occur when one of the dimensions that are transverse to the current bias direction is longer than the Josephson length ( $\lambda_J$ ), as given by

$$\lambda_J = \sqrt{\frac{\Phi_0}{2\pi\mu_0 d J_c}}, \quad (1)$$

where  $\Phi_0 = h/2e$  is the magnetic flux quantum,  $J_c$  is the critical current density and  $d$  is the magnetic thickness of the junction barrier [13], taking into account the London penetration depth in each electrode and the barrier thickness. The condition for this limitation is related to the current distribution. If the main part of the current is flowing on the edges of the strip constituting one JJ electrode, then the torque controlling the phase evolution (analogous to the current per unit length) is applied essentially at the ends of the JJ barrier. In such a case, the phase rotates locally at the ends of the barrier, and the required torque for further rotation becomes independent of the JJ length. Its critical current is not larger than the critical current density times the area occupied by the Josephson vortex:

$$I_{c,max} \approx J_c \cdot \lambda_J \cdot t_f, \quad (2)$$

where  $t_f$  is the width in the third dimension, for example, the thickness of a superconducting film with a bicrystal JJ. This also applies for parallel arrays of JJs, which can be seen as a discretization of an LJJ. Note that if the bias current were distributed uniformly, then the phase evolution would be the same all along the LJJ, restoring the proportionality of the critical current versus JJ length.

This reduction in the critical current ( $I_c$ ) by non-uniform current distribution degrades the response to magnetic fields because the voltage modulation increases with the  $R_n I_c$  product of the JJ, where  $R_n$  is the normal resistance and  $I_c$  is the critical current of the array. By increasing the number ( $N$ ) of JJs connected in parallel,  $R_n$  scales as  $1/N$ . Thus, it is at least necessary to keep the scaling of the critical current as  $N$  and, thus, to distribute the bias current uniformly. This is the basic reason for the structures we propose in this paper. We experimentally investigated a two-layer geometry [11] where the ground plane was replaced by a normal metal (Au) strip, with a width comparable to  $W$ . By changing the position of this second strip, we concluded that the critical current of a 21-JJ parallel array is maximum when the second strip is located right below the JJ array, corresponding to an optimal uniformity of the bias current.

In this paper, we investigate a possible improvement of this geometry, where both strips are replaced by a grid of strips. We show that the previously presented uniform current distribution is also expected in a system of two superimposed grids. Even though the current density is not uniform in each branch of the grid, the total current flowing in the grids is evenly distributed to each grid branch. As shown in Section 4.1, the alignment of the grids is not critical. Note that this principle can also be applied to a similar system in which series arrays of LJJs replace the 2D arrays, as in Figure 1c and reference [11]. We demonstrated a uniform current distribution and thus expect comparable performance, at least when the Josephson length ( $\lambda_J$ ) of the LJJs is large compared to the JJ spacing in the parallel array. Some of the potential advantages of this proposal are the following: (a) the response of a single array is improved by the uniformity of the bias current; (b) the removal of the limitation on array width (by self-field effects), as the new geometry of the field now enforces a uniform current distribution; (c) when two grids are one on top of the other, it is straightforward to double the amplitude of the response of the device using a series connection of the grids; (d) this last situation is obtained without increasing the surface of the device; and (e) the implementation is particularly suited to cases of an integrated multilayer technology and can also be considered in flip-chip or piggyback configurations.

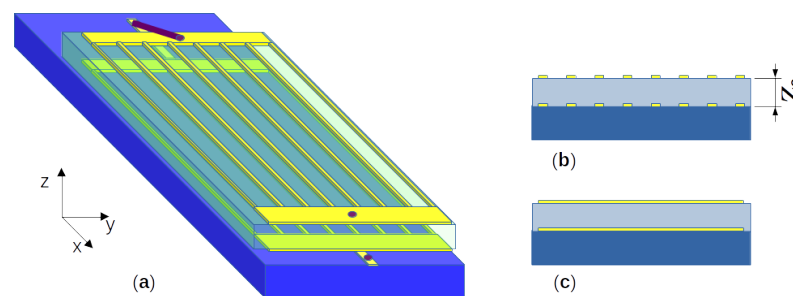


**Figure 1.** Schematic representation of the 2D array used in the model. (a) 3D perspective. (b) Section view for a grid. (c) Section view for a series array of LJJs.

### 3. Model

In our models, the devices are long enough in the direction of the current flow ( $x$ ) so that we can neglect the end effects and invariance along  $x$  can be assumed. Choosing the Coulomb gauge, the vector potential ( $A$ ) is also oriented along  $x$ , and the magnetic field is perpendicular to this direction. We used the finite element method implemented in FreeFEM++ software [14] to solve the only non-zero component of the potential vector,  $A_x$ , using the iterative algorithm presented by Alsop et al. [15]. In a system composed of two superconductors, they established the following set of equations:

$$\frac{\Phi_0 \nabla \phi_i}{\lambda^2} = \nabla^2 A_x - \frac{A_x}{\lambda^2} \quad (3)$$

where  $\nabla$  is the gradient operator, and  $\phi_i, i = 1, 2$  are the superconducting phases. Each is constant over the section of a superconducting branch of the grid, and as all branches

contained in the same layer are connected together at each end, this constant is common to the entire section of each grid, and its value is converging during the iterative computation.

We made a FreeFEM++ model of a 2D array of JJs such that half of the array is in a lower horizontal plane, while the other half is in the upper horizontal plane, as represented in Figure 1. The second half is a copy of the first half translated vertically by a quantity ( $z_h$ ). Later in this paper, we also consider the effect of a horizontal shift transverse to the current flow ( $y_2$ ); the current flows in the  $x$  direction, along the different branches of the grids. The orientation of the axes defined in Figure 1 applies to the whole content of this paper.

We assume that all the JJs connected in parallel are identical. We neglect the presence of the JJs in the evaluation of the current distribution for two reasons. First, the perturbation is nearly the same for identical JJs. Furthermore, secondly, the perturbation is comparable to a quadrupole, decaying with  $d_j$ , the distance from the JJs, as  $(d/d_j)^2$ , where  $d$  is the magnetic thickness of the JJ barrier (generally less than one micrometer). Thus, it affects the magnetic field distribution only to a minor extent. Neglecting this maintains invariance by translation at long distances ( $d_j$ ) from the JJs. The model invokes boundaries of the simulation space; we set  $A_x = 0$  at a distance approximately twice as large as the transverse dimensions of the device. Initial values of the superconducting phase gradient ( $\nabla\phi_i, i = 1, 2$ ) are opposite to be consistent with  $A_x = 0$  at a large distance and with opposite currents flowing in each layer. This is related to the geometrical symmetry and the equality of the self-inductances per unit length ( $\mathcal{L}$ ) in each array. As  $\nabla\phi_i$  is related to the fluxoid, it is proportional to the sum of the geometrical and kinetic inductances:

$$\mathcal{L} = \frac{\Phi_0 \cdot \nabla\phi_i}{I_i} \quad (4)$$

where  $I_i$  is the current in grid  $i$ . Conversely, having an educated guess of the inductance per unit length is equivalent to having suitable initial values such that 4 or 5 iterations lead to convergence (maximum relative change of  $A_x < 10^{-5}$ ).

## 4. Results

### 4.1. Micrometer-Scale Circuits

Figure 2a,b illustrate the results for a perfectly aligned array, with dimensions given in the legend. Besides the opposite values in each branch, we observe Figure 3 that the current density is larger close to the edges (and in a minor way, close to the surface) of the conductor, as expected from the Meissner effect in any wire. We define the branch current as the current density integrated over the section of one branch. Table 1 compares the calculated branch currents in the case of arrays with 7 and 11 parallel branches. They are very similar in each branch of the arrays: for the seven-branch array, departure from homogeneity is a deficit of 0.14% on the edges (outer pair of branches), and correspondingly, between 0.04 and 0.08% excess current on the inner branches. For the 11-branch array, there is a current deficit of 0.36% in the branches on the edges, a nearly ideal share of 1/11 in the next pair of branches and between 0.08 and 0.12% excess current in the inner branches. This indicates that for a parallel array of  $N$  JJs, each JJ receives nearly the same bias current, i.e., that the critical current of the array is close to  $N$  times the critical current of one JJ. Thus, the critical current for a wide parallel array is maximum, not limited by the self-field effect. As mentioned earlier, the same is expected for long JJs and long JJ arrays. The effect of the distance ( $z_h$ ) is comparable to the fringing effect in a two-plate capacitor; while  $z_h$  increases, the current tends to increase on the edges and to decrease in the center of the grid, as in the microstrip case. The realization of such a configuration is straightforward with low-critical-temperature technologies, where multilayer structures are employed. For high-critical-temperature (HTc) technologies, this possibility is much less common. Alternative solutions exist where the arrays are on different substrates and assembled together in a flip-chip or piggyback configuration. In principle, the distance ( $z_h$ ) separating the arrays should be smaller than the width of the arrays. For a flip-chip configuration,  $z_h$  is usually in the range of 20...50  $\mu\text{m}$ , i.e., suited for devices somewhat wider than the present limitation:

typically  $10\ \mu\text{m}$ . This value may be larger for smaller critical current densities, but it is not recommended to reduce the critical current because it reduces the Josephson energy. The distance ( $z_h$ ) is larger (in the range of  $100\ \mu\text{m}$  to  $1\ \text{mm}$ ) in the case of a piggyback assembly (because of the substrate thickness). This configuration is suitable only if the arrays are  $\sim 1\ \text{mm}$  wide. Such arrays would typically have hundreds of JJs in parallel and, in order to reach impedances of about  $10\ \Omega$ , would have thousands of JJs in series. Having hundreds of JJs in parallel would lead to critical currents above  $1\ \text{mA}$ . This may be an issue for proper configuration of the wires used to feed the current without creating a parasitic magnetic field but is still feasible. We also investigated the effect of a transverse shift ( $y_h$ ) on an 11-branch array, as reported Figure 4 and in the rightmost columns of Table 1. They show that an important shift can be tolerated; the departure from uniformity is now  $\sim 1.5\%$ . This allows for an implementation in a flip-chip (or piggyback) configuration.

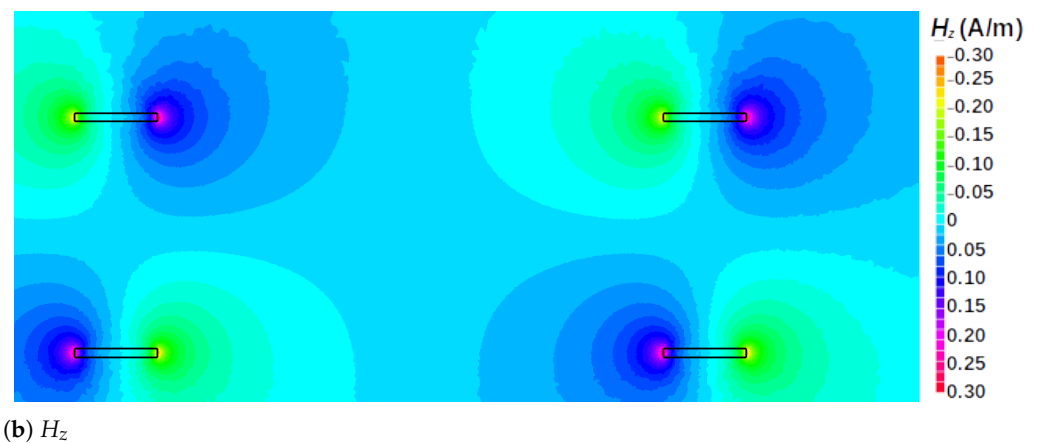
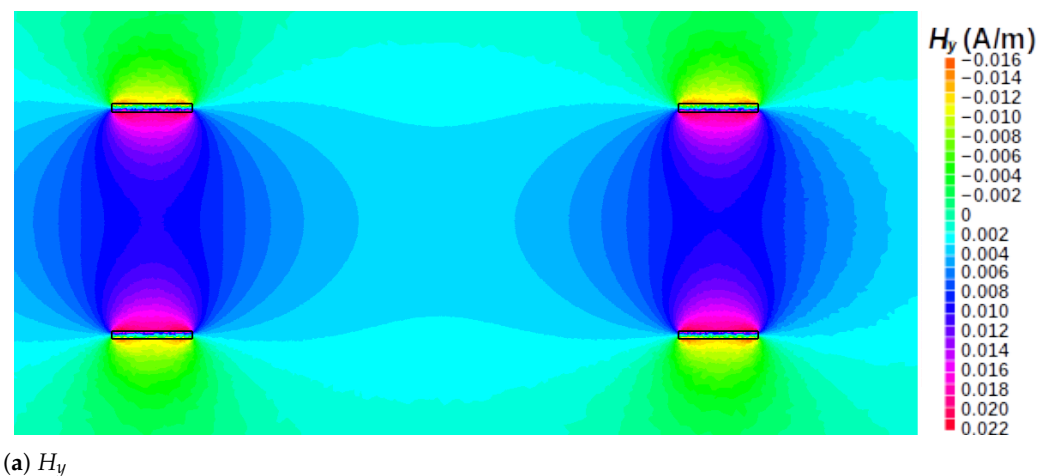


**Figure 2.** Maps of the magnetic excitation ( $H$ , in units of  $\text{A/m}$ ) in the section of the array. Black rectangles represent the edges of the superconducting strips. Their dimensions are  $1.4 \times 0.2\ \mu\text{m}^2$ , and their spacing is  $10\ \mu\text{m}$  horizontally and  $4\ \mu\text{m}$  vertically. (a)  $H_y$  and (b)  $H_z$ .



Figure 3. Current density in one branch in units of mA/μm<sup>2</sup> when the total current is 1 mA.

Table 1. Percentages of branch currents for arrays made with 7 (2 columns on the left) and 11 (4 columns on the right) parallel branches. In the 11-branch device, the effect of a transverse shift of half the pitch of the array is evaluated.

Branch Nbr.	Aligned		Aligned		$y_2 = 5 \mu\text{m}$	
	Upper Layer (%)	Lower Layer (%)	Upper Layer (%)	Lower Layer (%)	Upper Layer (%)	Lower Layer (%)
1	14.2654	−14.2654	9.05833	−9.05837	9.03718	−9.16116
2	14.2908	−14.2908	9.09035	−9.09033	9.08054	−9.09618
3	14.2955	−14.2955	9.09795	−9.09793	9.08699	−9.09087
4	14.2964	−14.2964	9.10092	−9.10092	9.08877	−9.08988
5	14.2955	−14.2955	9.10217	−9.10218	9.08928	−9.08975
6	14.2908	−14.2908	9.10263	−9.10261	9.08953	−9.8949
7	14.2654	−14.2654	9.10219	−9.10220	9.08976	−9.08934
8			9.10093	−9.10088	9.08992	−9.08879
9			9.09791	−9.09792	9.09076	−9.08695
10			9.0903	−9.09032	9.09619	−9.08045
11			9.05842	−9.05843	9.16116	−9.03722

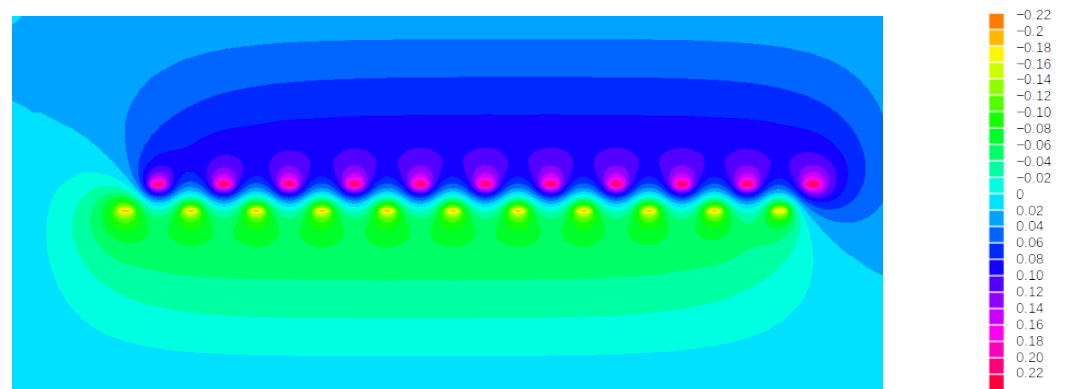
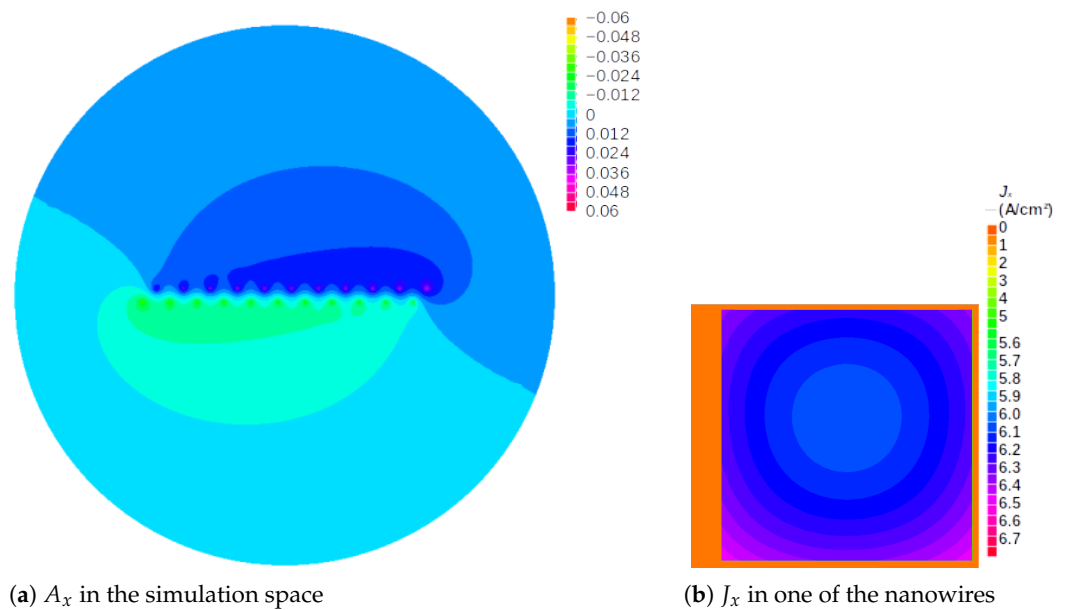


Figure 4. Map of the  $A_x$  component in the section view of a two-layer device with grids made of 11 “misaligned” branches, as they are horizontally shifted by 5 μm with respect to each other along the  $y$  direction. Units of the right scale are reduced to  $\mu_0$ .

#### 4.2. Submicrometer-Scale Circuits

We now investigate the suitability of this approach for nanostructures. We restrict ourselves to structures where the superconducting material has a coherence length much shorter than the dimensions of the device to avoid loss of coherence. This situation is generally encountered in high-temperature superconductors. The model does not account for potential variation of the pairing potential ( $\Delta(r)$ ). In Figure 5, the grids have a horizontal pitch of 1 μm, and the width of the grid branches is 100 nm. The film thickness is 100 nm,

and the vertical spacing between the layers is 500 nm. Again, we shifted the upper layer horizontally by 500 nm to investigate a misalignment effect. Figure 5a shows a map of  $A_x$  in the simulation space, and Figure 5b shows a map of  $J_x$  with an expanded view of a single grid branch from the top grid. For Niobium ( $\lambda = 0.135 \mu\text{m}$ ), the obtained value of inductance is  $0.52 \text{ pH}/\mu\text{m}$ . This includes the geometric inductance and the kinetic inductance. For the map of the current density, we used a non-uniform distribution of the iso-values in order to enhance the resolution inside the grid branch; the values separating the different domains (colors) are separated by 0.5 between 0 and  $5.5 \text{ A}/\text{cm}^2$  and by 0.05 between  $5.55$  and  $6.75 \text{ A}/\text{cm}^2$ . As one may expect, there is a minimum of current density close to the center of the nanowire. An asymmetry can be observed, with larger current densities in the lower part of the nanowire due to the other grid facing the lower side. Ideally, the current density is maximum on the edges of the superconductor, which can be observed as close as  $0.2 \text{ nm}$  from the edges, thanks to the good control on the mesh provided by the simulation software. The distribution of the current in each grid branch is given in Table 2. Again, the current distribution is almost uniform on the grid. This is not surprising for an overall width of only  $10 \mu\text{m}$ , as it is not very different from the distribution obtained in a conventional single-layer geometry. The same model for a grid of 61 nanowires, i.e.,  $60 \mu\text{m}$ -wide, produces a current distribution with a uniformity still better than 8%.



**Figure 5.** (a) Map of the  $A_x$  component in the section view of a two-layer device with units of the right scale reduced to  $\mu_0$ . (b) Enlarged section view on one of the grid branch (nanowire) showing the current density (note that the scale on the right is enlarged for the top 10%). The grids are made of 11 “misaligned” nanobranches, as they are horizontally shifted by  $0.5 \mu\text{m}$  with respect to each other along the  $y$  direction.

**Table 2.** Percentages of branch currents for arrays made with 11 parallel nanowires, showing the effect of a transverse shift of half the pitch of the array (0.5  $\mu\text{m}$ ).

Branch Nbr.	Upper Layer (%)	Lower Layer (%)
1	8.767	−9.388
2	8.948	−9.237
3	9.018	−9.168
4	9.055	−9.133
5	9.078	−9.113
6	9.095	−9.095
7	9.113	−9.078
8	9.133	−9.055
9	9.168	−9.018
10	9.237	−8.948
11	9.389	−8.767

#### 4.3. Dependence on Material Properties

Besides the critical temperature, the critical current density and the critical magnetic field, the main parameters characterizing the superconducting materials for this study are the London penetration depth ( $\lambda$ ) and the coherence length. As already mentioned in Section 4.2, our study focuses on devices with dimensions much larger than the coherence length, i.e., where this parameter has a negligible effect. We now check that this is also true for the London penetration depth on the 11-branch device with a misalignment of 5  $\mu\text{m}$  presented in Section 4.1.

Table 3 reports the current distribution in the different branches for two values of the London penetration depth. The results differ by less than 0.13% when  $\lambda$  is doubled. Obviously, this is expected, as the magnetic field only slightly depends on the current distribution in the wires (provided that the wire thickness is much smaller than the distance ( $z_h$ ) separating the two grids and that the wire width is much smaller than the grid pitch). For grids made of nanowires, where the nanowire dimensions are generally much smaller than the London penetration depth, independent of the superconducting material, the dependence of the results on the choice of material is expected to be much smaller.

**Table 3.** Percentages of branch currents for arrays made with 11 parallel wires, with a transverse shift of half the pitch of the array (0.5  $\mu\text{m}$ ). The leftmost columns are repeated from Table 1, corresponding to a penetration depth of 0.135  $\mu\text{m}$ . The rightmost columns correspond to a penetration depth of 0.27  $\mu\text{m}$ .

Branch Nbr.	$\lambda = 0.135 \mu\text{m}$		$\lambda = 0.27 \mu\text{m}$	
	Upper Layer (%)	Lower Layer (%)	Upper Layer (%)	Lower Layer (%)
1	9.03718	−9.16116	8.93331	−9.29025
2	9.08054	−9.09618	9.05521	−9.11825
3	9.08699	−9.09087	9.07706	−9.09461
4	9.08877	−9.08988	9.08333	−9.08884
5	9.08928	−9.08975	9.08542	−9.08744
6	9.08953	−9.8949	9.08642	−9.08638
7	9.08976	−9.08934	9.08746	−9.08556
8	9.08992	−9.08879	9.08904	−9.08339
9	9.09076	−9.08695	9.09424	−9.07695
10	9.09619	−9.08045	9.11827	−9.055
11	9.16116	−9.03722	9.29025	−8.93339

We believe that the principle can be extended to cases in which the coherence length is not smaller than the size of the conductors. The bias current distribution presents the same features, with quantitative changes. We expect that any dissipative effect that does not introduce magnetic-flux-dependent superconducting phase shifts will only contribute to a

better uniformity of the bias current distribution. Modeling this situation would require the insertion of Usadel's equations in the model, as previously performed, for example, by Khapaev et al. [16]. Note that the proposed two-plate geometry requires a non-zero critical current of the branches including the JJs in order to possibly improve the transfer factor of a magnetic field detector.

## 5. Discussion

Compared to the long-JJ case, the magnetic field for the grid (parallel array) case is nearly periodic along the  $y$  axis in both horizontal and vertical components. The spatial Fourier components are attenuated rapidly with distance and are not expected to change the uniformity of current distribution for the branches at first order. A possible effect of this shift on current distribution within each branch may occur but will be negligible with small JJs. If the arrays are periodic but with different pitches, we expect a "frequency beat" pattern of the current distribution in the grid with the smaller pitch.

We have presented results only for periodic grids, i.e., with equal spacing between the branches. In the case of non-periodic grids [6], we have to distinguish between identical arrays in the layers and the case of different arrays. In the first case, each branch is facing another branch, and both carry opposite currents. These currents are very similar to both the currents flowing in the wide microstrip case and in the periodic grid case presented above. The assumption that the array in one layer is identical to the array in the other layer is presumably not critical. The essential requirement is that their bias currents be opposite (and with a similar magnitude) and that the arrays have similar widths. In the case where  $z_h$  is clearly larger than the distance between two neighboring branches, the local magnetic field results from the contributions of several facing branches located in a region with a width of about  $z_h$ . As long as  $z_h$  is clearly larger than the maximum distance between two neighboring branches within each array, the uniformity of the current distribution in the different branches should not be affected. We expect degradation if a single branch in one grid is facing several branches of the other grid, again assuming that each branch contains the same JJ geometry. In summary, in order to keep some uniformity in the current distribution, we want to design arrays with equal values of the critical current densities integrated over a width of  $y_c \approx z_h$ .

For multilayer technologies, one may expect that the superconducting layers might not have the same superconducting properties. In particular, the London penetration depth might not be the same. However, the details of the current distribution in each grid branch have no importance in the "long range", i.e., a few microns away. We also expect that the film thicknesses are not critical as long as they are thin. Of course, if the dimensions of the grid elementary cell are large enough to allow for trapped flux quanta in the cell hole, this will destroy the uniformity of the current distribution. Obviously, an array entirely located in one layer, with the second layer containing a plain superconducting plane, should be more robust to flux trapping. However, it is very difficult couple external magnetic fields. Thus, a robust circuit may employ only resistive elements in the second layer, where the current distribution is imposed by the resistive nature of the material.

Finally, we note that for the nanodevice investigated herein, the value of the shift is only feasible with multilayer technologies. For flip-chip and piggyback technologies, the applicability is restricted to devices for which the shift value is much less than the width of the device. The advantages of using nanojunctions are the smaller magnetic field dependence of their critical current, their smaller bias current and their larger impedance.

## 6. Conclusions

The proposed two-layer structure implementing a return current as a "reversed image" in a second layer appears to bring the following advantages: (a) The bias current is uniformly distributed in the different branches of a parallel array of superconducting strips; (b) When two arrays are one on top of the other, it is straightforward to double the amplitude of the response of the device using a series connection of arrays; (c) This

last situation is obtained without increasing the surface of the device; (d) It eliminates the self-induced flux, thereby removing the limitation on array width. Preliminary results indicate that the device critical current is enhanced, i.e., approaches the maximum value given by the sum of individual JJ critical currents. More importantly, this should improve the response factor to the magnetic field of wide parallel arrays. This structure is acceptable for many technologies, as it can be either integrated or hybridized, and misalignment of the grids is not critical. It is applicable to many superconducting devices: arrays of long Josephson junctions connected in series, arrays of SQUIDs connected in series and 2D arrays of Josephson junctions. Based on our simulations, we think that this principle is not only applicable to short JJs and LJJs but also to nanojunctions.

## 7. Patents

The principle of uniform current distribution by mutual effect on two arrays is patented (PCT/EP2022/088070).

**Author Contributions:** Conceptualization, D.G.C.; methodology, Y.L.; formal analysis, D.G.C.; investigation, S.M. (Sarah Menouni) and J.K.; resources, C.U.; writing—original draft preparation, D.G.C. and S.M. (Salvatore Mesoraca); supervision, B.M.; project administration, J.T.; funding acquisition, D.G.C. and B.M. All authors have read and agreed to the published version of the manuscript.

**Funding:** This work was performed within the C2N micro nanotechnologies platform, partly supported by the French funding agencies CNRS (Centre National de la Recherche Scientifique/RENATECH network) and the General Council of Essonne, as well as by ANR (Agence Nationale de la Recherche) grant number 21-CE24-0023-02 (ARPEJ).

**Institutional Review Board Statement:** Not applicable.

**Informed Consent Statement:** Not applicable.

**Data Availability Statement:** Although most of the data presented in this paper were generated by simulation tools and can be reproduced independently, we agree to provide them upon reasonable request.

**Conflicts of Interest:** The authors declare no conflict of interest.

## Abbreviations

The following abbreviations are used in this manuscript:

MDPI	Multidisciplinary Digital Publishing Institute
DOAJ	Directory of open access journals
JJ	Josephson junction
LJJ	Long Josephson junction

## References

1. Clarke, J., Braginski, A.I. (Eds.) *The SQUID Handbook Vol. I: Fundamentals and Technology of SQUIDs and SQUID Systems*; Wiley-VCH Verlag GmbH & Co. KGaA: Weinheim, Germany, 2004.
2. Seidel, P. (Ed.) *Applied Superconductivity: Handbook on Devices and Applications*; Wiley: Weinheim, Germany, 2015.
3. Clarke, J. Superconducting quantum interference devices for low frequency measurements. In *Superconductor Applications: SQUIDs and Machines*; Schwartz, B.B., Foner, S., Eds.; Plenum: New York, NY, USA, 1977.
4. Vettoliere, A.; Silvestrini, P.; Granata, C. Superconducting quantum magnetic sensing. In *Quantum Materials, Devices, and Applications*; Henini, M., Oliveira Rodrigues, M., Eds.; Elsevier: Amsterdam, The Netherlands, 2023. [\[CrossRef\]](#)
5. Cybart, S.A.; Herr, A.; Kornev, V.; Foley, C.P. Do multiple Josephson junctions make better devices? *Supercond. Sci. Technol.* **2017**, *30*, 090201. [\[CrossRef\]](#)
6. Oppenländer, J.; Caputo, P.; Häussler, C.; Träuble, T.; Tomes, J.; Friesch, A.; Schopohl, N. Effects of magnetic field on two-dimensional superconducting quantum interference filters. *Appl. Phys. Lett.* **2003**, *83*, 969–971. [\[CrossRef\]](#)
7. Drung, D.; Assmann, C.; Beyer, J.; Peters, M.; Ruede, F.; Schurig, T. DC SQUID Readout Electronics With Up to 100 MHz Closed-Loop Bandwidth. *IEEE Trans. Appl. Supercond.* **2005**, *15*, 777–780. [\[CrossRef\]](#)
8. Kornev, V.K.; Kolotinskiy, N.V.; Skripka, V.A.; Sharafiev, A.V.; Mukhanov, O.A. Output power and loading of superconducting quantum array. *IEEE Trans. Appl. Supercond.* **2015**, *25*, 1602005. [\[CrossRef\]](#)
9. Mitchell, E.E.; Müller, K.-H.; Purches, W.E.; Keenan, S.T.; Lewis, C.J.; Foley, C.P. Quantum interference effects in 1D parallel high-Tc SQUID arrays with finite inductance. *Supercond. Sci. Technol.* **2019**, *32*, 124002. [\[CrossRef\]](#)

10. Oswald, D. Current and current density distribution in parallel superconducting wires in a planar array in the Meissner state. *Cryogenics* **1973**, *13*, 290–298. [[CrossRef](#)]
11. Crété, D.; Lemaître, Y.; Marcilhac, B.; Trastoy, J.; Ulysse, C. Effect of self-induced flux in parallel arrays of Josephson junctions. In Proceedings of the IEEE International Superconductive Electronics Conference (ISEC), Riverside, CA, USA, 28 July–1 August 2019; pp. 1–3. [[CrossRef](#)]
12. Barone, A.; Paternò, G. *Physics and Applications of the Josephson Effect*, 2nd ed.; J. Wiley & Sons: New York, NY, USA, 1982; Chapter 5.
13. Weihnacht, M. Influence of Film Thickness on D.C. Josephson Current. *Phys. Status Solidi B*. **1969**, *32*, 169–172. [[CrossRef](#)]
14. FreeFEM++. Available online: <https://freefem.org/> (accessed on 23 May 2023).
15. Alsop, L.E.; Goodman, A.S.; Gustavson, F.G.; Miranker, W.L. A Numerical Solution of a Model for a Superconductor Field Problem. *J. Comput. Phys.* **1979**, *31*, 216–239. [[CrossRef](#)]
16. Khapaev, M.M.; Kupriyanov, M.Y.; Bakurskiy, S.V.; Klenov, N.V.; Soloviev, I.I. Modeling Superconductor SFN-Structures Using the Finite Element Method. *Differ. Equat.* **2020**, *56*, 959–967. [[CrossRef](#)]

**Disclaimer/Publisher’s Note:** The statements, opinions and data contained in all publications are solely those of the individual author(s) and contributor(s) and not of MDPI and/or the editor(s). MDPI and/or the editor(s) disclaim responsibility for any injury to people or property resulting from any ideas, methods, instructions or products referred to in the content.